Atomic-scale dynamics of a model glass-forming metallic liquid: Dynamical crossover, dynamical decoupling, and dynamical clustering

Abhishek Jaiswal,[1] Takeshi Egami,[2] and Yang Zhang[1,3,*]

[1]*Department of Nuclear, Plasma and Radiological Engineering, University of Illinois at Urbana-Champaign, Urbana, Illinois 61801, USA*

[2]*Department of Materials Science and Engineering, Department of Physics and Astronomy, University of Tennessee, Knoxville, Tennessee 37996, USA*

[3]*Department of Materials Science and Engineering, University of Illinois at Urbana-Champaign, Urbana, Illinois 61801, USA*

(Received 6 February 2015; revised manuscript received 5 April 2015; published 20 April 2015)

The phase behavior of multicomponent metallic liquids is exceedingly complex because of the convoluted many-body and many-elemental interactions. Herein, we present systematic studies of the dynamical aspects of a model ternary metallic liquid $Cu_{40}Zr_{51}Al_9$ using molecular dynamics simulations with embedded atom method. We observed a dynamical crossover from Arrhenius to super-Arrhenius behavior in the transport properties (self diffusion coefficient, self relaxation time, and shear viscosity) bordered at $T_x \sim 1300$ K. Unlike in many molecular and macromolecular liquids, this crossover phenomenon occurs well above the melting point of the system ($T_m \sim 900$ K) in the equilibrium liquid state; and the crossover temperature T_x is roughly twice of the glass-transition temperature of the system (T_g). Below T_x, we found the elemental dynamics decoupled and the Stokes-Einstein relation broke down, indicating the onset of heterogeneous spatially correlated dynamics in the system mediated by dynamic communications among local configurational excitations. To directly characterize and visualize the correlated dynamics, we employed a nonparametric, unsupervised machine learning technique and identified dynamical clusters of atoms with similar atomic mobility. The revealed average dynamical cluster size shows an accelerated increase below T_x and mimics the trend observed in other ensemble averaged quantities that are commonly used to quantify the spatially heterogeneous dynamics such as the non-Gaussian parameter α_2 and the four-point correlation function χ_4.

DOI: 10.1103/PhysRevB.91.134204 PACS number(s): 64.70.pe, 61.20.Lc, 66.10.−x, 66.20.−d

I. INTRODUCTION

Novel disordered alloys of various high entropic forms have attracted much attention from physicists and materials scientists over the past few decades. Because of the lack of long range crystalline order, bulk metallic glasses (BMG), as prominent examples, show many unusual properties, such as remarkable mechanical strengths and stiffness, excellent wear and corrosion resistance, very high coefficient of restitution, near-net-shape casting, biocompatibility, and soft magnetic properties. Consequently, they are favorable candidates in a broad range of applications [1–9].

Recent interests in BMGs center around Copper and Zirconium based glassy alloys, which exhibit excellent glass-forming abilities [2,10,11]. They have shown to form stable glasses for a wide variety of compositions. Yet, one of the ensuing challenges to mainstream utilization of such BMGs remains the inability to manufacture them in even larger sizes and better qualities, required for advanced engineering applications [3,10,12]. BMGs are usually produced by quenching high-temperature multicomponent metallic liquids to room temperature at a sufficiently fast rate such that local crystallizations are suppressed in the frozen states. While many efforts have been devoted to exploring combinations of materials to form stable metallic glasses [13–17] as well as microstructure analysis, it is believed that understanding the fundamental aspects of the liquid state dynamics of these melts still holds the key to understanding their glass-forming abilities.

In addition, multicomponent metallic liquids and glasses can serve as interesting model systems to study how many-body and many-elemental interactions manifest themselves on the way to the thermodynamically unstable but kinetically trapped states [6,18–20]. With regards to such glassy materials, the general consensus is that a glass transition occurs when the relaxation process slows down by several orders of magnitude while the structure remains almost unchanged. A plethora of theories have been proposed to underpin the mechanisms of glass transition of simple unitary or binary liquids that interact via straight-forward pair potentials [21–26]. In particular, in light of wisdoms learned from critical phenomena, many recent theoretical developments have focused on searching for an appropriate nonequilibrium "order parameter" counterpart to describe the glass transition [27–30]. Such attempts propose to use the size of dynamic heterogeneity, an idea borrowed from spin glasses, as a "dynamic" correlation length that can potentially quantify the glass transition [20,31,32]. However, there remain significant challenges in terms of (1) to what extent these theories can be applied to describe the complex multicomponent metallic liquids and their glass transitions, and (2) the understanding of the mechanisms responsible for enhancing the glass-forming ability. Despite these complications, one advantage of metallic liquids and glasses as interesting model systems is the absence of complex internal degrees of freedom that are omnipresent in other molecular and macromolecular glass formers [2,6,10].

The liquid state is usually characterized by local structure and dynamics, both self and collective. Neutron scattering, alongside computer simulations, has been the frontier tool in

*To whom correspondence should be addressed: zhyang@illinois.edu

investigating liquids [33–35]. Hence our understanding and descriptions of the statistical quantities in liquid state are formulated in the framework of space and time correlation functions and can be directly probed by neutron scattering experiments. Computer simulations, on the other hand, have helped obtain deeper insights of the liquid state of materials by comparing with experimental measurements. Metallic liquids can be relatively reliably studied using classical molecular dynamics (MD) simulations on large systems accelerated by use of classical many-body interaction potentials.

There have been several other studies performed using MD simulations on Cu-, Zr-, and Al-based metallic glasses in liquid, supercooled, and glassy states [13,15,16,36–40]. The embedded atom method (EAM) force field [36] has been extensively used in studying these ternary systems. The emphasis of many previous studies has been on quantifying the structural orderings in the melted and glassy states [40,41] and predicting structure-property correlations in such BMGs [5,37,42–45]. The formation of an icosahedronlike structure has been quantified both computationally and experimentally. The importance of localized interactions and bond formation between Al and Cu has been elucidated with regards to this key structural motif. It has also been reported that these structural signatures of the fragility only exists in deeply supercooled Cu-Zr liquids [46–48]. Besides structure and thermodynamics, the dynamics also plays a key role in the properties of BMGs. Studies of liquid-state dynamics are mostly limited to binary systems. In the supercooled state, it has been proposed that a fragile-to-strong crossover can be observed via decoupling of diffusion coefficient and relaxation time [49]. In another study, a binary system with composition ($Cu_{33.3}Zr_{66.7}$), the Stokes-Einstein relation is found to break down in the liquid state [50]. However, there are qualitative assertions on the mechanism underlying this behavior without much detailed emphasis on its physical picture. A detailed study of the liquid state dynamics in such multicomponent metallic systems is lacking. Several experimental measurements of dynamics in liquid and supercooled state have been performed using electrostatically levitated droplets in inelastic neutron scattering facilities [51–55]. By and large, such measured systems are ternary or higher in composition and thus, there is a pressing need to study them using reliable potentials to develop greater insights from such experiments.

In this paper, we address these concerns by studying a model system compositionally similar to a BMG manufactured by Liquidmetal® Technologies, Inc., namely, LM601 ($Zr_{51}Cu_{36}Ni_4Al_9$). Ni is very similar in size to Cu, and from a dynamical point of view has very similar diffusional characteristics. Thus the system studied using MD, $Cu_{40}Zr_{51}Al_9$, could mimic the quaternary BMG appropriately. We use the ternary EAM potential to study the structure and self-motions of the constituent elements in this model system. The paper is organized as follows: we begin by describing the structure of this system in terms of the pair correlation functions and the static structure factor. This is followed by descriptions of dynamical quantities such as mean-squared displacement, self van Hove correlation functions, self-intermediate scattering functions, etc. Investigations of the self-motions led to testing the validity of Stokes-Einstein relation in this glass-forming metallic liquid. In the following discussions, we focus on an emerging concept, heterogeneous dynamics and our novel methodology to visualize and quantify it in a 3D system using a nonparametric unsupervised machine-learning technique. We conclude our discussions by relating a few statistical quantities that probe the nature of this heterogeneity to the concepts of onset of correlated dynamics in the system and demonstrate the agreement with results from the machine-learning technique.

II. METHODS

Molecular dynamics (MD) simulations were carried out using the open-source parallel simulator LAMMPS [56], developed by the Sandia National Laboratory. At first, we attempted to model the exact quaternary system LM601, with the EAM potential obtained by rapid fitting techniques [57]. However, the system resulted in a gel-like mixture that eventually phase-separated within the equilibrium liquid. Furthermore, to the knowledge of the authors, there are no other available potentials developed for quaternary systems comprising the elements used in this quaternary BMG. Thereafter, we carried out MD simulations using a relevant EAM potential for the ternary Cu-Zr-Al system. For more details on the EAM potential, readers are referred to Ref. [36]. The system size is 100 000 atoms (51 000 Zr, 40 000 Cu, and 9000 Al) in a cubic box. Periodic boundary conditions were enforced in all three dimensions. The system was heated up to a temperature of 2500 K and well equilibrated for 100 ps at zero external pressure (NPT ensemble with a Nosé-Hoover thermostat) to obtain the correct volume. The system was then cooled to subsequent temperatures with a cooling rate of 10 K/ps in the range of 950–2500 K, which are higher than the reported melting temperature of the system, ∼900 K. The system was allowed to evolve for another 100 ps after it cooled down to the required temperature. In this equilibrium state, the system is not expected to show any aging effects, as the system is fast relaxing. Once the system was fully equilibrated at a given temperature, NPT ensemble was enforced to generate the trajectory outputs and to compute relevant statistical quantities. Relevant ensemble averaged quantities such as the mean-squared displacement, self-intermediate scattering functions, etc., were computed by averaging over a large subset of trajectory snapshots.

Subsequent dynamical cluster analysis was performed in a smaller system of 4,000 atoms with the same relative composition of each element. This was done with a conscious effort to easily demonstrate the method's usability and produce quick and clear visualizations. Displacement of individual particles between a time scale of the structural relaxation time at any specified temperature was used to quantify the characteristic dynamics in the liquid. During the structural relaxation time window, the average displacement of atoms is roughly between the $g(r)$ first peak and the first valley [58,59]. The distribution of the displacements was divided into smaller bins or "mobility groups" ranging from 15–1000 bins. Particles were classified into each of these mobility groups based on their displacements. Particles in one mobility group were used to further perform an hierarchical clustering analysis (HCA) using a nonparametric, unsupervised machine-learning algorithm [60,61]. This algorithm sorts data by creating binary clusters that join to form a larger cluster in a hierarchical

level dendrogram based on natural groupings in the data. The first step involves characterizing the dis/similarity between every pair of data in the set using Euclidian distance measures. Solitary data points, identified as isolated particles with no other particles within two diameters of the largest atom Zr, are filtered out at this step to enhance the robustness of the algorithm. Reduced data points with close proximity are grouped in binary pairs and form a hierarchical tree spanning the entire set of data points. To find natural groupings in this tree, an inconsistency coefficient [60–62], which ranges from 0 to 2 and characterizes each link of the cluster tree by comparing its heights with the mean height of all other links at the same level of hierarchy, was used with an optimized value 1.0 throughout all analysis. The value of 1.0 was so chosen to ensure distances between objects joining a (binary) cluster are similar to the distance of the particles in that (binary) cluster. A higher inconsistency value indicates the clusters are much farther than the distances of the constituent particles of each clusters and thus defines a natural clustering set. The mean cluster size, defined as the average number of particles in a cluster for each mobility group, was computed by averaging over all clusters, including the isolated single particles filtered in an earlier step. To understand the size of these dynamical clusters, the entire system was further regrouped into five major groups and their trends, etc., were studied. A minimal spanning tree [63–65] was used to draw connections between atoms that form a networking cluster.

III. RESULTS AND DISCUSSIONS

A. Structure

At first, the structure of the material represented by the pair distribution functions $g(r)$ and the total static structure factor $S(Q)$ was routinely checked. The amorphous nature of the system in the liquid states was verified. No sharp transitions can be appreciated throughout the studied temperature range from these static quantities.

1. Pair distribution function

For an isotropic and homogenous liquid system, the pair distribution function (PDF) or radial distribution function (RDF), depends only on the modulus of relative atomic distance and can be computed as follows:

$$g(r) = \frac{1}{4\pi r^2 \rho N} \left\langle \sum_{l \neq l'} \delta(\mathbf{r} - |\mathbf{r}_l - \mathbf{r}_{l'}|) \right\rangle. \qquad (1)$$

Partial $g(r)$ for the six possible pairings were computed by discretizing the cubic simulation cell into small concentric volumetric regions, counting the respective atom pair types and subsequently normalizing the counts by the volume of the spherical shells. The amorphous nature of the system is clearly illustrated in Fig. 1, along with the nearly homogenous mixing of atoms in the system. The results are consistent with those published by the developers of the potential in Ref. [36] differing only in the intensity of peaks due to the temperature and composition differences. The Al-Al correlation is found to be the weakest owing to its lowest composition and it is suggestive of being inside local cages formed by Cu and Zr atoms. Zr favors ordering with Al atoms, as indicated by the highest intensity of the partial $g(r)$.

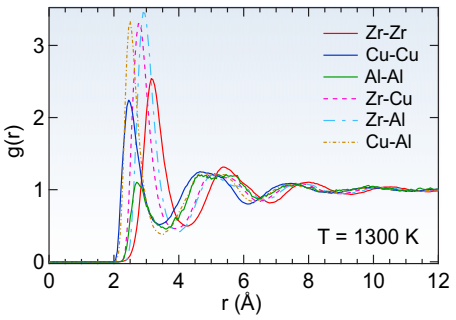

FIG. 1. (Color online) Partial $g(r)$ derived using EAM potential for $Cu_{40}Zr_{51}Al_9$ metallic liquids at 1300 K. Al-Al correlation is weak suggesting caging by Cu and Zr atoms.

2. Structure factor

The static structure factor $S(Q)$ is a quantity that can be directly measured by scattering experiments such as with neutrons or x rays. For an isotropic system there are no preferred orientation and hence the structure factor depends only on the modulus of the wave vector transfer Q. The experimentally measured structure factor by neutrons is weighed by the proper coherent bound neutron scattering lengths "b" and needs to be factored in when computing the total $S(Q)$ of the system as shown:

$$S(Q) = \frac{1}{N\langle b \rangle^2} \left\langle \sum_{l,l'=1}^{N} b_l b_{l'} \exp\{-i\mathbf{Q} \cdot [\mathbf{r}_l - \mathbf{r}_{l'}]\} \right\rangle. \qquad (2)$$

A simplified representation of $S(Q)$ is shown in Eq. (3). In performing the computations of $S(Q)$, the computational complexity of Eq. (2) is reduced to $\mathcal{O}(N)$ by performing angular averaging over 500 random angular directions using Eq. (3). Figure 2(a) shows the temperature dependence of $S(Q)$

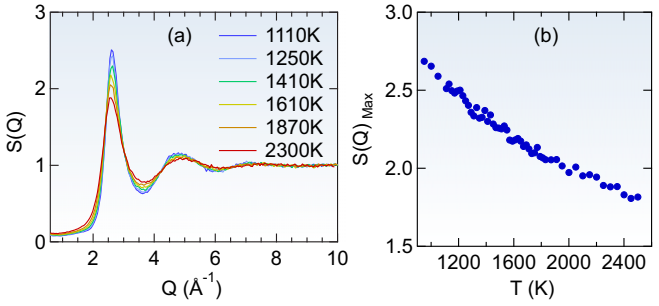

FIG. 2. (Color online) (a) Temperature evolution of the total neutron structure factor $S(Q)$ of $Cu_{40}Zr_{51}Al_9$ system. (b) The first peak position of $S(Q)$ shows a continuous temperature dependence.

representative of a normal liquid state:

$$S(Q) = \frac{1}{N\langle b\rangle^2}\left\langle\left[\sum_{l=1}^{N} b_l \cos(\mathbf{Q}\cdot\mathbf{r}_l)\right]^2 + \left[\sum_{l=1}^{N} b_l \sin(\mathbf{Q}\cdot\mathbf{r}_l)\right]^2\right\rangle. \quad (3)$$

The peak position of the first $S(Q)$ peak is approximately 2.6 Å^{-1} and is found to shift in both intensity and position with increasing temperature. Subsequent computations of wave-vector dependent quantities are computed at this Q value, which is roughly representative of the scale of the first peak in the $g(r)$ of the system. This peak position in $S(Q)$ is proportional to changes in the atomic density of the material. Any evidence of structural changes observed in the temperature range used in the experiments may be employed to explain the phase transition behavior that has been observed in many metallic liquid systems. A monotonically decreasing peak amplitude [Fig. 2(b)] is observed in the temperature range without the presence of any distinct structural order change. Structural analysis reveals a smooth temperature dependence without any sharp transitions.

B. Dynamics

The major focus of this work concerns the investigation of the self-dynamics of constituent elements of this glass-forming metallic liquid. Single-particle dynamics, evidently influenced by neighboring atoms, of the multicomponent liquids involves multiple relaxations and long-time diffusions. Statistical quantities that illustrate liquid dynamics can be studied in both real space and time or in the reciprocal (Fourier) space. To this end, we begin by illustrating the self van Hove correlation function and then move on to other time and space correlation functions.

1. Self van Hove correlation function

The motion of a single particle can be studied using the self-part of the van Hove correlation function [66,67]. In the liquid state, the system is isotropic and hence these quantities depend only on the magnitude of displacements not their directions,

$$G_s(r,t) = \frac{1}{N}\left\langle\sum_{l=1}^{N}\delta(\mathbf{r}+\mathbf{r}_l(0)-\mathbf{r}_l(t))\right\rangle. \quad (4)$$

At $t = 0$, the $G_s(r,t)$ has a singularity at the origin indicative of the particle under investigation. The physical meaning of $G_s(r,t)$ is the probability of finding a particle i in the vicinity of some distance "r" at some other time "t" given that it was at the origin at $t = 0$. In essence, it describes the average motion of such a particle. The volume integral of $G_s(r,t)$ is a conserved quantity and equals unity. Hence, in Fig. 3, we plot the quantity $4\pi r^2 G_s(r,t)$ for all constituent particles at a high and a low temperature value. The intensity of the color map in the insets corresponds to the time and location of finding a particle with certain probability. This probability distribution is found to broaden with increasing time, evidenced by the widening colored regime. As expected, individual particles are observed to diffuse much faster at

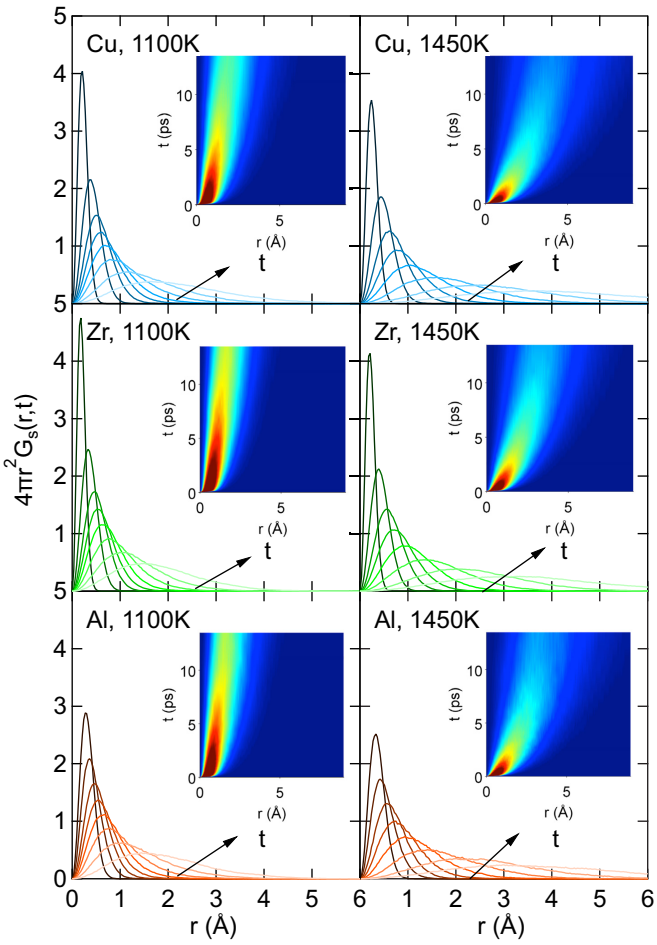

FIG. 3. (Color online) $G_s(r,t)$ normalized by the area to measure the probability distribution of finding a particle at a later time. As expected, all three species in the system exhibit a hydrodynamic behavior with a single Gaussian peak that broadens in spatial direction with increasing time at 1450 K. However, at 1100 K, the Gaussian behavior is slightly distorted. At 1450 K, the particle diffuses much faster than at 1100 K evidenced by the broadening of the distribution. Insets show normalized $G_s(r,t)$ in both "r" and "t" directions.

1450 K than at 1100 K. In the temperature range studied, the particles show distributions for a normal liquid without the presence of any prominent secondary peaks. Usually, when the system gets close to the glass transition, multiple peaks may appear in the probability distributions that have been attributed to the thermally activated hopping process [68]. The time taken for correlations to decay to the hydrodynamic limit or Gaussian behavior is generally comparable to the structural relaxation time of each species in the liquid state [58]. The non-Gaussian behavior of $G_s(r,t)$ at intermediate time scale is discussed later in the paper.

2. Mean-squared displacement and self-diffusion coefficient

The mean-squared displacement of particles at an elapsed time t is related to the second moment of the self van Hove

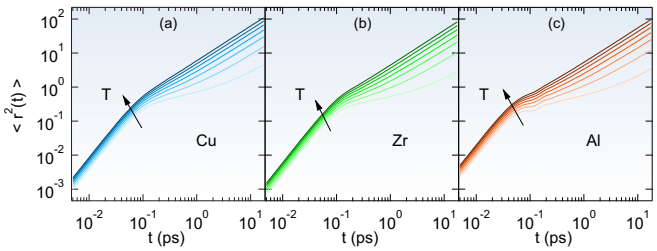

FIG. 4. (Color online) Temperature dependence of mean-squared displacements (MSD) for constituent elements. Arrow indicates increasing temperature. Al shows largest displacements at short times compared to Zr and Cu.

correlation function [34,35],

$$\langle r^2(t)\rangle = \frac{1}{N}\left\langle \sum_{l=1}^{N} |\mathbf{r}_l(t) - \mathbf{r}_l(0)|^2 \right\rangle = \int r^2 G_s(\mathbf{r},t)d\mathbf{r}. \quad (5)$$

The computational implementation of mean-squared displacements (MSD) involves averaging of particle displacements over all particles of interest at two time points. It is a measure of the average distance traveled by a particle. At short times, particles show ballistic motions, i.e., a particle does not encounter any other particles in its vicinity. In this case, the distance traveled is linearly proportional to the time interval considered, and thus MSD is proportional to t^2. Usually, the time scale for this behavior is indicative of the mean free time. Beyond the ballistic motions, there is a plateau that is much more pronounced at lower temperatures and indicative of the onset of a caging effect. This is roughly equivalent to the time needed for a local configurational or topological excitation in the system [69]. At longer times, particles collide with one another and eventually undergo a random walk. In this regime, MSD is linearly proportional to t. Consequently, the self-diffusion coefficient can be computed directly in MD simulations using the MSD of each atom,

$$D = \lim_{t\to\infty} \frac{1}{6t}\langle |\mathbf{r}_i(t) - \mathbf{r}_i(0)|^2\rangle. \quad (6)$$

Al being the lightest element in the system shows much larger displacements at short times as shown in Fig. 4(c). In contrast, at long time, the MSD of Cu is the largest, and that of Zr is the smallest. Such elemental features can be further studied from the long-time self-diffusion coefficient of each atom extracted from a linear fit of the MSD at long time. Cu shows the largest diffusion coefficient while Zr is the slowest among the elements. Temperature dependence of the self-diffusion coefficient can be described by many models such as Arrhenius, VFT, MCT, parabolic, free-volume, Adam-Gibbs, etc. In this analysis, we did not try to fit the entire temperature range with any particular model, but focused on the deviation from the Arrhenius behavior (Fig. 5). Therefore we applied an Arrhenius fit at high temperatures to extract the activation energy E_A and diffusion constant D_0 for each element. A sharp deviation from the Arrhenius fits is observed around $T_x \sim 1300$ K, which is much higher than the melting temperature of the system (~900 K). This is indicative of the onset of correlated dynamics of the system, where system transitions from a state with the uncorrelated

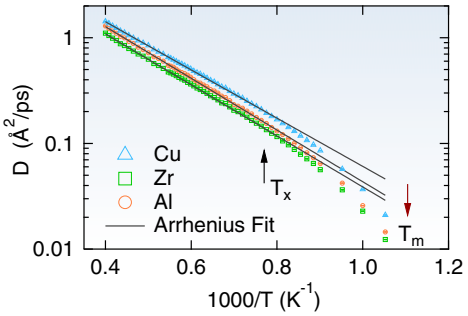

FIG. 5. (Color online) Self-diffusion coefficients extracted from MSD for each element. Black arrow ($T_x \sim 1300$ K) indicates the onset of correlated dynamics (crossover) marked by a deviation from the respective Arrhenius fits. Red arrow indicates the melting temperature of this system ($T_m \sim 900$ K).

liquid dynamics at very high temperatures to a state with increasing cooperativity in various regions in time and space [69]. For most molecular systems, this deviation from the Arrhenius law usually happens below the melting point in the supercooled regime, and therefore has raised some concerns on whether the system is well equilibrated in the simulation studies. As this study is concerned with temperatures much higher than the glass transition, there are no effects due to aging. In the multicomponent metallic liquids, the chemical disorder essentially pushes the dynamical crossover higher than the melting point, resulting in a noncontroversial equilibrium phenomenon. The addition of Al in slowing down the dynamics of Cu-Zr based liquid has been discussed elsewhere [70]. Hence the additional chemical disorder brought by Al addition can be responsible for the observation of dynamical crossover above T_m. Furthermore, it is interesting to note that the dynamical crossover temperature is more or less the same for all three constituent elements. As the local structure in various spatial regions is comprised of an Al center with Cu-Zr atoms as neighbors, their local cooperativity necessarily influences the manifestation of a dynamical crossover in each element.

3. *Self-intermediate scattering function*

The atomic trajectories obtained from the MD simulation provide comprehensive information to compute the self-intermediate scattering functions (SISF). SISF is defined as the spatial Fourier transform of $G_s(r,t)$ to the reciprocal space, which can be measured either directly by correlation spectroscopy and neutron spin echo technique, or indirectly by inelastic scattering experiments:

$$F_s(Q,t) = \frac{1}{N}\left\langle \sum_{l=1}^{N} \exp\{-i\mathbf{Q}\cdot[\mathbf{r}_l(t) - \mathbf{r}_l(0)]\}\right\rangle. \quad (7)$$

The Intermediate Scattering Function (ISF) is thus named as it can be Fourier transformed in time to obtain the dynamic structure factor $S(Q,\omega)$ or inverse Fourier transformed in space to recover the van Hove correlation function $G(r,t)$. SISF characterizes the density fluctuations of the same particle in the system at time $t = 0$ and at another subsequent time t. Figure 6 shows the temperature dependence of SISF for each

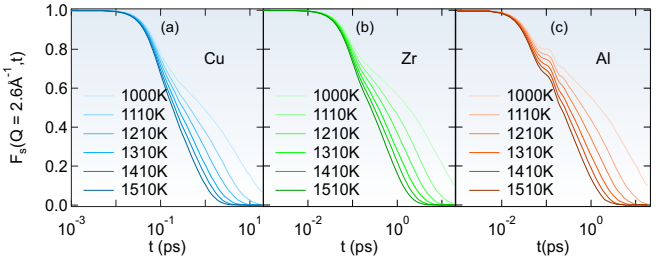

FIG. 6. (Color online) Self-intermediate scattering functions $F_s(Q,t)$ of the constituent elements of a $Cu_{40}Zr_{51}Al_9$ metallic liquid system at $Q = 2.6$ Å^{-1}. Cu and Zr atoms show simple two-step relaxations, while Al shows additional peaks around 0.1 ps.

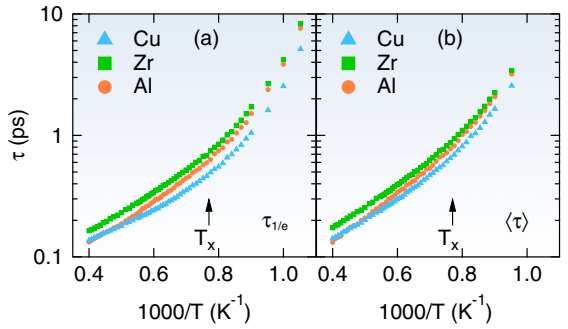

FIG. 7. (Color online) Angell plot of temperature dependence of τ_α. (a) τ found using a $1/e$ cut of SISF. (b) $\langle\tau\rangle$ computed by the area under SISF. Al transitions from fast Cu-like dynamics at high T, to much slower Zr-like dynamics at low T.

constituent element. For dense liquids, the decay of SISF can roughly be separated into two steps: fast cage breaking of atoms and the subsequent slow diffusion of the atoms [71]. SISF shows a Gaussian-like behavior at short times indicative of ballistic or vibration motions of particles followed by multiple step relaxation processes in the subpicosecond to picosecond time scale. At low temperatures, SISF is highly stretched and reveals two relaxation mechanisms separated by a shoulder corresponding to the plateau in MSD. The early relaxations are usually referred as the β-relaxation regime. A slower relaxation process referred as the α-relaxation follows the subsequent shoulder in $F_s(Q,t)$.

The α-relaxation time is usually defined as the time needed for $F_s(Q,t)$ at the first peak $Q = 2.6$ Å^{-1} of the structure factor $S(Q)$ to decay to $1/e$ [34,35]. Recent studies highlight that in high temperature liquids the α-relaxation time τ_α is roughly three times the time scale needed for a local configurational excitation or a bond-breaking/forming event $\tau_{\rm LC}$. τ_α also corresponds to the average time for an atom to move a distance of the interatomic distance [59]. The temperature dependence of τ_α is found to be similar to that of $\tau_{\rm LC}$, τ_B, (bond lifetime) and τ_M (Maxwell relaxation time, discussed later on). The bond lifetime τ_B is defined as the average time for an atom to lose half of the neighbors. An alternative definition of the average relaxation time, which is quite frequently used in experiments, is the area under the $F_s(Q,t)$ curve. This definition of the average relaxation time also takes the short and intermediate time behaviors into account, and therefore its value and curvature in the Angell plot are slightly different from those of the relaxation time defined by the $1/e$ cut of the $F_s(Q,t)$. Further discussions can be found in Ref. [72]:

$$\langle\tau\rangle = \int_0^\infty F_s(Q,t)dt. \tag{8}$$

Care must be given to note a full decay of $F_s(Q,t)$ before applying this definition. With increasing temperature, atomic mobility is increased leading to a reduction in relaxation time. The deviation from a simple Arrhenius behavior (linear) is easily observed in Figs. 7(a) and 7(b) plotted in a semilogarithmic scale. Just like the self-diffusion coefficient, this activated nature of temperature dependence of τ_α can be described with various functional forms. In fact, in the temperature range we studied, the data can be fit well with most of the models. However, despite various fittings of the activated dynamics, a deviation of τ_α from the Arrhenius behavior is observed around $T_x \sim 1300$ K and agrees with what has been reported in other studies [69]. Extracting fast relaxation time (β relaxation) from SISF is usually sensitive to model fittings and the time range used, and as such cannot be relied upon.

It is interesting to note that Al has much faster dynamics at high temperatures similar to Cu but slows down considerably and behaves like Zr in relaxation time scales at lower temperatures. We may thus interpret that Al atoms couple to faster Cu atoms at high temperatures, but switch to slower Zr atoms at lower temperatures. It has been suggested that Al addition to this system greatly improves the glass-forming ability of Cu-Zr based metallic liquids. The mechanisms responsible for this improvement still remain elusive. In the glassy state, Al favors the formation of icosahedral structural ordering with improved symmetry, connectivity, and charge stability via bonded interactions [70]. In the liquid state, the striking slowing down of dynamics with Al coupling to Zr-like dynamics can partially be responsible for such improvements. Q dependence of SISF allows computations of relaxation time at various length scales. In the hydrodynamic limit, $Q \to 0$, τ, and the self-diffusion coefficient D are inversely related. Therefore the slope of the inverse of τ versus Q^2 plot in the small Q limit also gives the self-diffusion coefficient, which agrees with that extracted from MSD. Figure 8 shows the temperature dependence of inverse of τ versus Q^2 depicting the linear dependence for $Q < 1.7$ Å^{-1}.

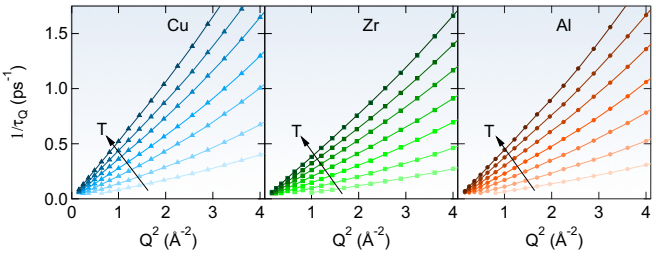

FIG. 8. (Color online) Inverse of structural relaxation time τ_α plotted against Q^2 shows a linear dependence for small Q values. The slope of the curve, when fitted with a linear curve, can be used to extract the self-diffusion coefficient D.

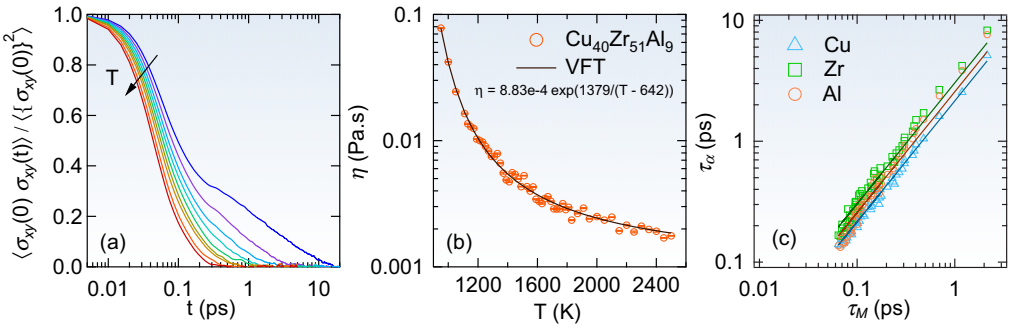

FIG. 9. (Color online) (a) Normalized stress autocorrelation function of melted $Cu_{40}Zr_{51}Al_9$ at various temperatures. (b) The computed shear viscosity of liquid $Cu_{40}Zr_{51}Al_9$ using the Green-Kubo relation and the temperature dependence is fitted using a VFT type equation. (c) Testing linearity between Maxwell relation τ_M and alpha relaxation time τ_α. τ_α is roughly three times of τ_M.

4. Shear viscosity

The shear viscosity is another key transport property describing the macroscopic liquid state dynamics, and can be calculated by equilibrium molecular dynamics (MD) calculations using the appropriate Green-Kubo relation [34,35]:

$$\eta = \frac{V}{k_B T}\int_0^\infty dt\,\langle\sigma_{xy}(0)\sigma_{xy}(t)\rangle, \tag{9}$$

where σ_{xy} is the off-diagonal x-y component of the stress tensor, k_B is the Boltzmann constant, V is the volume of liquid, and T is the absolute temperature of the system. In the framework of a very simple viscoelastic Maxwell model, a material undergoing shear exhibits exponential relaxation/decay of local stress with a characteristic relaxation time τ_M that is related to viscosity through the Maxwell relation.

$$\tau_M = \frac{\eta}{G_\infty}, \tag{10}$$

where G_∞ is the instantaneous (high-frequency) modulus of rigidity [35]. This relaxation behavior essentially separates the time scale where the system evolves from solidlike to liquidlike. In the framework of local configurational excitations, the viscosity of the system is a manifestation of elementary changes in the atomic connectivity network. Because the time scale for such local bond exchange and the time scale for stress relaxation are equal at high temperatures, it is postulated that the macroscopic stress is determined by the topology of the local neighbors of an atom [69]. The normalized shear stress autocorrelation function is a temperature dependent, monotonically decreasing function as shown in Fig. 9(a). At higher temperatures, shear relaxation is almost exponential while on approaching the melting point the relaxation becomes highly nonexponential. Decreasing temperature rapidly increases the correlation time and interestingly develops a "bump" around 0.3 ps. This feature has been attributed to effect of boson peak vibrations in the glassy state [50]. The shear viscosity obtained using the Green-Kubo relation is shown in Fig. 9(b) and fitted with a VFT (Volger-Fulcher-Tammann) equation. The temperature dependence of the viscosity can be fitted equally well using other models such as MCT, parabolic, etc. in the studied temperature range. The resulting fitting parameters depend on the temperature range we choose to analyze. Nevertheless, here we show the VFT fitting applied to the entire temperature range we studied as it results in the fitting parameter of interest, the diverging temperature, $T_0 = 642$ K, close to the reported glass transition for this composition. We demonstrate linearity between τ_α and τ_M by applying a linear fit in Fig. 9(c).

C. Dynamical decoupling

1. Decoupling of elemental dynamics

The self-dynamics of elements occurs in varying time scale in the system. This can be readily quantified by taking the ratios of elemental self-diffusion coefficients and the relaxation time shown in Fig. 10. Al and Zr diffusion and relaxations are observed to couple across the temperature range studied. Interestingly, this ratio reveals that Cu dynamics is clearly decoupled from both Al and Zr, and this decoupling is accelerated below the dynamical crossover temperature T_x. Local bond formations between Al and Zr atoms must promote their similarity. This decoupling of dynamics can be an important mechanism causing heterogeneous dynamics in the system in the liquid state. Rapidly decoupled elemental dynamics below T_x promotes spatial domains with distinct dynamics.

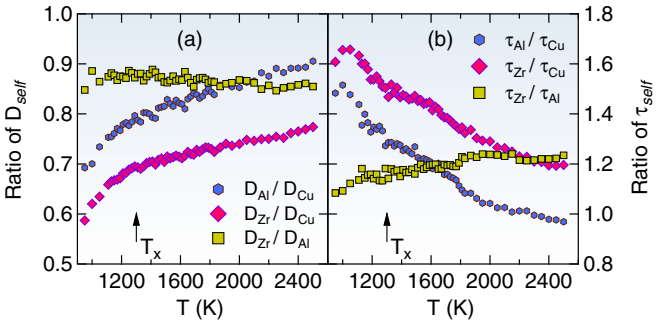

FIG. 10. (Color online) Decoupling of elemental dynamics revealed by taking the (a) ratio of self-diffusion coefficients and (b) ratio of α-relaxation time of all three elements. Al and Zr dynamics is highly coupled while Cu shows decoupling in the entire temperature range but accelerated below $T_x \sim 1300$ K.

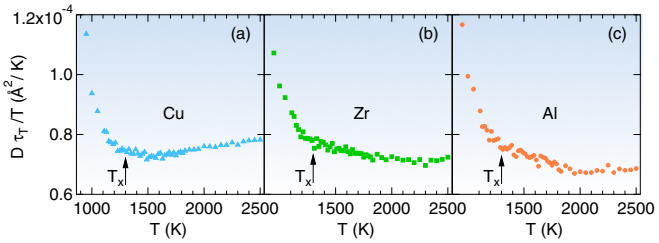

FIG. 11. (Color online) Breakdown of Stokes-Einstein relation is observed below $T_x \sim 1300$ K, which is well above the glass transition temperature of the system, and above the melting temperature of the system. The arrow indicates the onset temperature T_x where the dynamics crossovers from the uncorrelated to the correlated state.

2. Breakdown of Stokes-Einstein relation

Having computed both self-structural relaxation time and diffusion coefficient, we can test the validity of Stokes-Einstein relation (SER) in this glass forming liquid. SER relates the translational diffusion coefficient D, bulk viscosity η, and temperature T as $D \propto T/\eta$, and usually works well for high temperature liquids [73]. As viscosity η, Maxwell relaxation time τ_M, and α-relaxation time τ_α are proportional to each other, it is possible to study the validity of SER in such metallic melts using D and τ_α. We plot the quantity $D\tau_\alpha/T$ as a function of temperature in Fig. 11. At high temperatures, this quantity is approximately constant but increases sharply below $T_x \sim 1300$ K. Clearly, the deviations from the Arrhenius behavior of diffusion coefficient and relaxation time transpire to the breakdown of the SER in this metallic liquid at around $T_x \sim 1300$ K, which is sufficiently higher than its melting temperature. Results from this analysis illustrate the deviations in Arrhenius behavior of elemental diffusion and relaxation more distinctly.

In many liquids, a breakdown of SER is observed in the supercooled states but still above the glass transition temperature and have been empirically found to obey Fractional Stokes-Einstein relation [74,75] $D \propto (\tau/T)^{-\xi}$. Specifically, in several molecular and macromolecular liquids, this crossover behavior is observed around $\sim 1.2T_g$ [76]. The reported glass transition temperature T_g for this composition is approximately around 640 K. It is thus a surprising revelation that this crossover temperature T_x is roughly $\sim 2T_g$ and thus in the equilibrium liquid state. The many-body and complex chemical interactions among the alloying elements should be partly responsible for this behavior. In addition, many studies have attributed this violation of SER to the occurrence of dynamical heterogeneities in structural glass formers [77]. Dynamic heterogeneity, or spatially heterogeneous dynamics, refers to the existence of clusters of atoms, typically of the size of several particles (intermediate length scale) [78,79], whose relaxation dynamics differ from other nearby clusters. Such heterogeneities in liquids are consequences of highly mobile molecules forming clusters and moving cooperatively. These spatially correlated clusters allow local structural relaxations. Thus, due to the presence of clusters of varying local dynamics, the system as a whole cannot relax. Thus, in this liquid, such heterogeneous domains grow spatially and lead to a decoupling of translational diffusion and structural relaxation time.

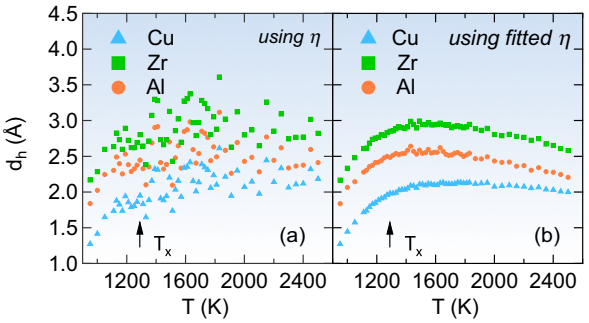

FIG. 12. (Color online) Effective hydrodynamic/Stokes-Einstein diameter of Cu, Zr, and Al using (a) viscosity η and respective self-diffusion coefficients D (b) using VFT fitted η. Clearly, at higher temperatures, the effective diameter is constant, while it is decreasing sharply below the dynamical crossover temperature T_x.

In high-temperature metallic liquids, the role of atomic configurations and stresses in connection to the dynamical onset or the landscape influenced regime has been discussed previously [58,69,80,81]. Local configurational excitations (LCE) [69], which involve the formation or breaking of a bond between neighbors, have been described as steps to change the atomic connectivity network and control structural relaxations in the system. In this landscape-influenced regime, LCE's are believed to interact via the dynamic long-range stress fields they create. Dynamic communications between two or more LCE's are thus involved in the flow mechanism. Such LCE's interactions may give rise to a spatially heterogeneous dynamics in the system [69]. However, the connections between these two mechanisms need to be studied further. Above the dynamical crossover temperature T_x, the time involved in LCE event and the Maxwell relaxation time agree with each other. This is suggested to explain the Arrhenius dependency of viscosity at high temperatures.

The effective hydrodynamic diameters of a liquid particle undergoing diffusion can be computed by utilizing the "slip" boundary condition [50]:

$$d_h = \frac{k_B T}{2\pi\eta D}. \tag{11}$$

This provides a rigorous meaning to the Stokes-Einstein relation and for it to hold, d_h, must be a temperature independent constant. At high temperatures, it is nearly a constant value while it sharply decreases below the identified onset of correlated dynamics (Fig. 12). The reduction of the effective diameter is indicative of local bond formations and development of correlations among particles.

D. Dynamical clustering

1. Dynamical cluster analysis using machine learning

In a multicomponent system, the spatially heterogeneous dynamics is believed to be initiated by the varying mobility of each species that form clusters and move cooperatively. While, many studies have resorted to computations of a "dynamical correlation length" using four-point correlation functions [27,28,82], a physical picture in the atomic scale is

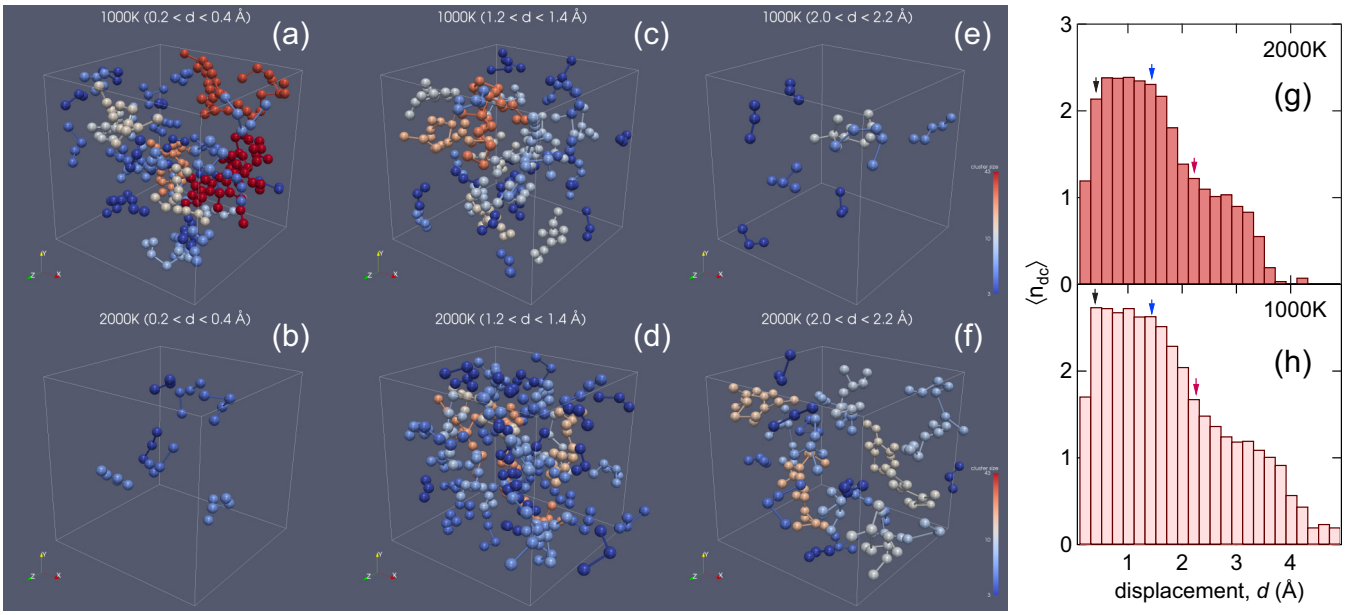

FIG. 13. (Color online) (a)–(f) Visualization of dynamical clusters with more than two atoms in each group, which are classified based on displacement of atoms over a time period of α-relaxation time at 1000 and 2000 K. In this analysis, distribution of displacements is divided into 25 bins and average cluster size in each mobility group is shown in (g) and (h). Clusters are colored by the number of atoms in groups (3–43 atoms). Larger clusters are formed at lower temperatures in the slow and intermediate mobility groups. Faster mobility groups do not show appreciable changes over the temperature range.

yet not fully developed beyond model 2D systems. Because of the highly localized nature of cooperative dynamics, it is necessary to establish relevant quantity that distinguishes local fluctuations in particle positions and velocities [83]. To quantify such a dynamical quantity, we choose the distribution of particle displacements over a time scale of structural relaxation as a measure of relevant dynamics.

We used a nonparametric, unsupervised machine learning technique to perform an automated cluster analysis. Cluster size analysis algorithm, as described in the methods sections, groups particles with very similar mobility into spatial clusters. The distribution of particle displacements at any temperature follows a Maxwell-Boltzmann type distribution, such that many particles have small to intermediate displacements. Few particles in the systems have very large displacements but their numbers increase with increasing temperature in the system. We choose τ_α as the time scale for performing this analysis because the range of displacements of particles is similar (in the range of 0–5 Å) and of the order of nearest neighbor distance for highly mobile particles, similar to collective jumps in soft-sphere glass in Ref. [84]. Another control parameter critical to this analysis is the number of mobility groups (bins) covering the distribution of displacements. Using a small bin number leads to larger number of particles in each mobility group. Subsequently, the sizes of clusters are larger simply due to availability of many particles in each group. Hence, in our analysis, the number of bins was varied from 20–1000 and verified to show no qualitative effect on the cluster size trend. However, with a large number of bins, the mean cluster sizes are smaller as each group contains fewer particles. For visualization purposes, 25 bins are used; while for temperature dependency, an optimal value of 250 bins is used to define the mobility groups for the 4000 particles.

In Fig. 13, clusters with more than two atoms are visualized for three different mobility groups indicated by the arrows in (g) and (h) at 1000 and 2000 K. Atoms within one cluster are connected via a minimal spanning tree for visual aid. Evidently, slower groups at 1000 K show the largest cluster sizes with up to 43 atoms. Intermediate mobility groups show comparable statistics at both temperatures. Faster atom numbers grow significantly at 2000 K leading to a larger number of clusters but no real size increase in comparison to those at 1000 K. To gain better insight into the temperature dependence of cluster size distributions, all 250 mobility groups are rearranged into five main groups with equal number of particles (20% in each group). We plot the mean size variation $\langle n_{\rm dc}\rangle$ across three of these five groups and the average (solid circle) over entire mobility groups versus temperature in Fig. 14. Single particles and pairs were also incorporated in this analysis. The size of dynamical clusters revealed by this machine learning technique follows the trends of $D\tau_\alpha/T$ (Fig. 11). At higher temperatures, evidently, there are clusters with fewer particles while below the identified dynamical crossover T_x the increase in the mean cluster size is more pronounced. For highly mobile clusters, the increase in size is very small. This is expected for such mobile clusters that span spatial regions in a transient manner. Furthermore, due to increase in particle number at smaller displacements at low temperatures, a large number of bins span 20% of the fastest particles. As the classification of five representative groups is based on a fixed number of atoms, each of these bins contains less particles. Hence the mean cluster size of fast groups remains small at low temperatures. While this feature is statistically controlled and can be analyzed using alternative approaches, it is more important to appreciate the general trend of increasing cluster sizes found in all other four groups and $\langle n_{\rm dc}\rangle$ with lowering temperature.

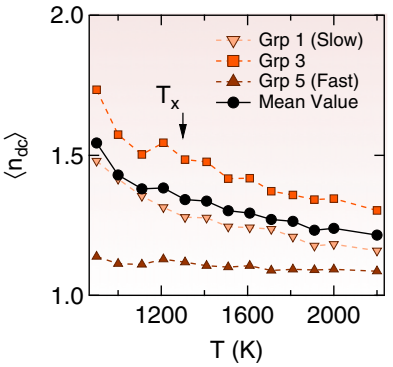

FIG. 14. (Color online) Mean number of atoms in dynamical clusters $\langle n_{\rm dc}\rangle$ classified into five major groups. Clearly, cluster size increases with decreasing temperature, but it increases sharply below the dynamical crossover temperature $T_x \sim 1300$ K. This feature is observed across all five groups as well as the mean value for each temperature. Average cluster size computation includes single particles. Displacement distribution is divided into 250 bins and average cluster size for each bin (or mobility group) is computed. Next, the slowest 20% of atoms are classified as Grp 1 (slow) particles, while the most mobile 20% are in Grp 5.

The quantified increase in cluster size in Fig. 14 spans a range of 1.0–1.8 atoms per group. While this may not seem a rapid increase numerically, it must be emphasized that this computation incorporates all the isolated single particles. The system still being a high temperature liquid, is highly mobile and as such, the clustering tendency is suppressed, unlike in supercooled states where cluster sizes have been reported to be much larger. Furthermore, it is important to clarify that the definition of a cluster is not unique and may be sensitive to the mobility parameter used [85,86]. This nonparametric technique reveals the atomic-scale spatial picture of increasing cooperativity of dynamically similar particles. Coexistence of clusters of mobile and immobile particles is a direct indication of heterogeneous dynamics. Within one cluster, in order for the structural relaxation to occur, all the particles have to coordinate with each other and find a way to rearrange themselves. As a consequence, the process needs to overcome a certain energy barrier, which gives rise to the slow dynamics. At high enough temperatures, each cluster is, in principle, composed of only one single particle, therefore, the dynamic correlation length should be close to one; while as the system is increasingly cooled, such clusters start to form and grow in size, therefore, the mean cluster size also increases. The crossover temperature T_x marks the onset of such correlated motions or dynamic heterogeneity.

In high-temperature metallic liquids, the role of atomic configurations and stresses characterized by local configurational excitation (LCE) has been discussed with regards to dynamical onset and glass transition [58,69,80,81]. Phonons in liquids are short-lived, strongly scattered and thus, can not be used to explain macroscopic dynamical properties. LCE, on the other hand, are linked to the macroscopic viscosity and could form the basis of elementary excitations in liquids. It is claimed that interactions of multiple LCEs may give rise to spatially heterogeneous dynamics in the system. Each LCE event involves breaking or formation of a bond. Thus the dynamic communication between LCEs involves 2–3 atoms. The average cluster size revealed by our technique 1–1.8 is influenced by many isolated, single particles. If such particles are filtered out, the mean size is in the range of 2–3 atoms and thus agrees with the LCEs picture.

In many relevant works, the underlying potential energy landscape that characterize the structural relaxations in the system is proposed to influence the nonexponential relaxations in liquids. In this landscape-influenced regime [68,87], the relaxation is found to be increasingly nonexponential in time. The temperature dependence of relaxations also deviates sharply from Arrhenius behavior. This corresponds to the liquid being able to sample deeper potential energy minima [69]. Hence, to cross these deeper energy barriers, requires the rearrangement of positions of several particles in different clusters independently. Thus the mechanism illustrated in our analysis also agrees with the qualitative assertions of energy landscape. To our knowledge, this is the first attempt at visualizing such dynamical clusters using advanced machine learning and nonparametric statistical analysis. Furthermore, in the ensuing sections, we show the agreement in trends with other commonly used measures of dynamic heterogeneity. Unlike the atomic scale measure of heterogeneous dynamics revealed by our analysis, these quantities are ensemble averaged over many possible configurations of the liquid.

2. *Non-Gaussian parameter*

The non-Gaussian parameter $\alpha_2(t)$ has been extensively used by researchers as a measure of dynamic heterogeneity:

$$\alpha_2(t) = \frac{3\left\langle \sum_{l=1}^{N} [\mathbf{r}_l(t) - \mathbf{r}_l(0)]^4 \right\rangle}{5\left\langle \sum_{l=1}^{N} [\mathbf{r}_l(t) - \mathbf{r}_l(0)]^2 \right\rangle^2} - 1. \qquad (12)$$

The computed $\alpha_2(t)$ in the temperature range of 950–2500 K are shown in Figs. 15(a)–15(c). For an isotropic system undergoing diffusive motions, MSD is linearly proportional to time and the van Hove self-correlation function is Gaussian in nature. As expected, $\alpha_2(t)$ is zero in this case. This is also true for short time ballistic motions of atoms in the cage where the velocity of atoms is described the Maxwell-Boltzmann distribution [88]. At intermediate times, $\alpha_2(t)$ is found to obey a power-law dependence on time given by $\alpha_2(t) \propto \sqrt{t}$ similar to observations in Ref. [89]. It is observed that $\alpha_2(t)$ usually peaks at a time corresponding to the crossover between the cage regime and the longer-time diffusive regime of the MSD. This time scale is in the late β regime. This is indicative of the fact that $\alpha_2(t)$ yields information on transiently mobile particles that jump due to the destruction of their cages [21]. A positive value of $\alpha_2(t)$ indicates that the probability for a particle to move very far is enhanced relative to a Gaussian random walk process [90]. While $\alpha_2(t)$ does not provide any information on the length scale, it is commonly observed to correlate with the time scale of maximal dynamic heterogeneity in the system.

The peak height of $\alpha_2(t)$ [Fig. 16(a)] when plotted against the temperature scale shows a similar behavior as $\langle n_{\rm dc}\rangle$ as well as the quantity $D\tau_\alpha/T$. It is approximately constant at high temperatures and shows a sharp rise around $T_x \sim 1300$ K. In this Cu-Zr-Al system, $\alpha_2(t)$ shows an uncharacteristic short time peak for Al even at very high temperatures. The time scale of this peak corresponds to that of oscillations in both

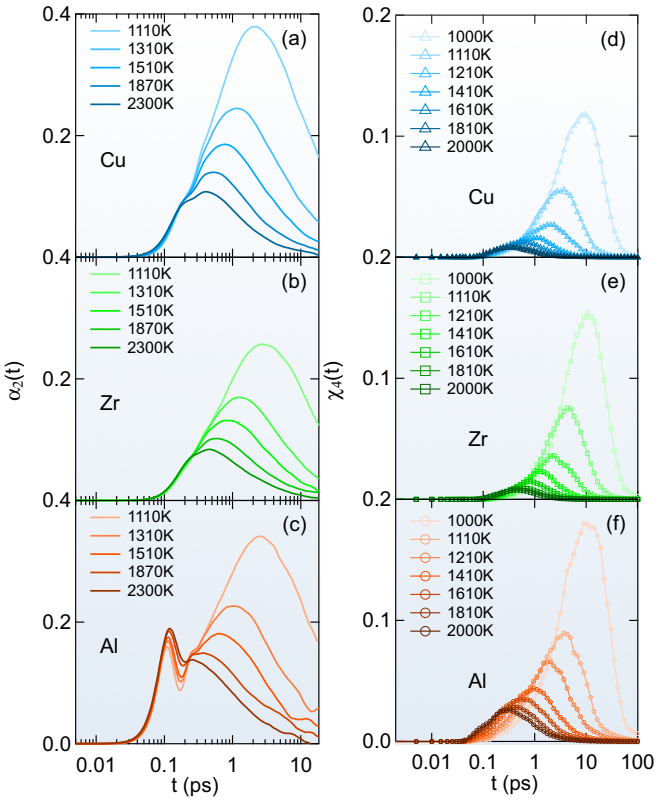

FIG. 15. (Color online) (a)–(c) Non-Gaussian parameter $\alpha_2(t)$ for constituent elements spanning a temperature range of 1100–2300 K. Al shows a distinct short time peak below the main structural relaxation time. This behavior is consistent with medium time scale oscillations in $F_s(Q,t)$ and MSD of Al. (d)–(f) Temperature dependence of four point correlation function $\chi_4(t)$ of constituent elements [27]. As T decreases, both $\alpha_2(t)$ and $\chi_4(t)$ increase in peak height and shift to a larger time value.

the MSD and SISF of Al. While the mechanisms behind this observation need further examination, an interesting consequence of this additional heterogeneity can be that the material is locally resistant to enhanced diffusions under conditions of localized heating or energy deposition. We hypothesize that the additional heterogeneity brought about by Al can lead to a resistance increase in the effective temperature in the glassy state.

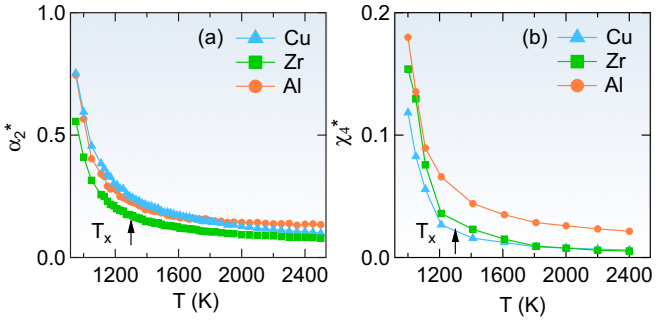

FIG. 16. (Color online) (a) The peak value of $\alpha_2(t)$, denoted as α_2^*, shows a distinct increase below the dynamical crossover temperature. (b) χ_4^* is defined as the maximum of $\chi_4(t)$. The temperature dependence of χ_4^* shows similar behavior as that of α_2^*, the mean cluster size $\langle n_{\rm dc}\rangle$, and $D\tau_\alpha/T$. Arrows indicate the dynamical crossover temperature $T_x \sim 1300$ K.

3. *Four-point correlation function*

In highly viscous liquids approaching glass transition, the relaxation spectra span a wide range of time and are strongly nonexponential [20,78]. The characterization of the spatial fluctuations dynamics of the system must be resolved in both space and time and also their variance from average behavior. A direct quantification of the length scale characterizing the motion of correlated particles in liquids involves the motion of two or more particles, hence, we use a four-point, time-dependent density correlation function that contains information about the density at two spatial points and two times [27,82]:

$$\chi_4(t) = \frac{V}{TN^2}\left[\left\langle Q_s^2(t)\right\rangle - \langle Q_s(t)\rangle^2\right],$$
$$Q_s(t) = \sum_{l=1}^{N} w(|\mathbf{r}_l(t) - \mathbf{r}_l(0)|). \tag{13}$$

To capture the correlated motions between particles in liquids, we used a "coarse graining" approach by utilizing an "overlap" function that measures overlap between configurations at time $t = 0$ and a future time t, described in Ref. [27]. The overlap function $w(|r_1 - r_2|)$ is unity for $|r_1 - r_2| \leqslant a$ and 0 otherwise. The distance parameter "a" is chosen to be larger than the square root of the plateau of MSD. Using a value of $a = 1.0$ Å, $\chi_4(t)$ was computed in the temperature range of 950–2500 K and shown in Figs. 15(d)–15(f). Contribution to $\chi_4(t)$ comes from localized particles (self correlations) and particles that move and are replaced by other particles (distinct). It is shown that self-correlations dominate the $\chi_4(t)$ suggesting increasing contributions of localized particle fluctuations. Hence, only self-correlations were assessed in computations of $\chi_4(t)$.

The qualitative behavior of $\chi_4(t)$ has been described by many authors [27,28,82,91,92]; at very short times $t = 0$ and long times $t = \infty$, $\chi_4(t)$ is close to zero, while in between it shows a peak around a time scale of the order of typical relaxation time of the liquid. It is believed that such time dependence reflects the transient nature of heterogeneous dynamics 28. Peak height of $\chi_4(t)$, denoted by χ_4^*, is interpreted as the correlated volume for structural relaxations, or simply an average "size" of dynamic heterogeneity. Studying the temperature variation of χ_4^* in this model glass forming system reveals increasing spatial correlations of dynamics in all constituent elements below the identified dynamical crossover. Figure 16(b) reveals the drastic increase in peak height χ_4^* below $T_x \sim 1300$ K in Cu, Zr, and Al. While the qualitative features of $\chi_4(t)$ agree for all three elements in the liquid, there are subtle variations in the time scale of peak value and in the χ_4^*. Al shows the largest scale of correlations among all elements, which could be indicative of correlations in dynamics and spatial structural fluctuations. The time scale of χ_4^* can also be used as a measure of the structural relaxation time of the liquid.

IV. CONCLUSIONS

In this paper, we characterize the equilibrium liquid state of a model multicomponent metallic liquid system, displaying complex many-body interactions, using molecular dynamics simulations, with emphasis on incoherent or self-motions of constituent elements. The structure of the liquid behaves similar to a simple liquid but reveals locally favored bonding among Al and Zr atoms. Subsequent analysis of dynamic quantities reveals a deviation from the Arrhenius behavior below a crossover temperature $T_x \sim 1300 \pm 100$ K, which is well above its melting temperature of $T_m \sim 900$ K and roughly twice of the glass-transition temperature of the system. Below T_x, the dynamics of Cu atoms is found to decouple strongly from that of Al and Zr atoms. In addition, the Stokes-Einstein relation that relates the diffusion coefficient and the macroscopic shear viscosity or structural relaxation time also breaks down in the equilibrium liquid phase at T_x. The mechanisms for such decoupling are interpreted as the increase in spatially heterogeneous dynamics or development of intermittent correlated rearranging regions mediated by the dynamic communications among local configurational or topological excitations. The many-body and chemical complexity of the investigated metallic liquid allows the examination of these phenomena unambiguously in the equilibrium liquid state. The onset of sluggish dynamics at such a high temperature temptingly suggests that this material can be a good-glass former. The incipience of cooperativity in the equilibrium state marks a sudden increase in dynamical cluster formation. As the system is systematically cooled below the liquidus temperature, we expect that the dynamical clustering trend will enhance. However, upon reaching close to the experimental glass transition, it can only be qualitatively asserted that such correlation lengths may span the entire system length.

To obtain an atomic-scale understanding of the spatially correlated dynamics, we use a nonparametric, unsupervised machine-learning algorithm to find natural clusters of particles with similar mobility at the time scale of structural relaxation. The method allows unambiguous direct visualization of three-dimensional dynamical clusters. Results from this cluster analysis reveal that the dynamical cluster size progressively increases with decreasing temperature, but below the dynamical crossover temperature T_x this phenomenon is accelerated among particles with slow to intermediate mobility. Particles with the largest mobility do not show any appreciable increase in cluster sizes. This is expected because such mobile particles do not span any spatial domain for a long period and can be isolated due to their enhanced mobility. This cluster analysis technique is qualitatively insensitive to the number of mobility groups used in the analysis. The temperature-trend of cluster size increase matches that of other commonly used measures of dynamic heterogeneity such as non-Gaussian parameter $\alpha_2(t)$ and four-point correlation functions $\chi_4(t)$. The effective hydrodynamic radius also reveals a drastic decrease in size below T_x. This agreement reveals that the method is able to provide a compelling picture of the dynamic heterogeneity. This technique can be further extended to characterize the morphology of the clusters, the influence of element types on cluster formation and time-evolution of dynamical clusters.

ACKNOWLEDGMENTS

We thank LiquidMetal® Technologies, in particular Stephanie O'Keeffe, Joseph Stevick, and Glenton Jelbert, for revealing us the details of the LM601 sample that formed the material basis of these simulation work and for providing LM601 sample measured in the neutron scattering experiments (to be published). We appreciate helpful discussions with Herbert R. Schober and David Chandler. AJ and YZ are supported by NRC faculty development award NRC-HQ-12-G-38-0072 and UIUC Campus Research Board Award RB14187. TE is supported by the U.S. Department of Energy, Office of Science, Basic Energy Sciences, Materials Science and Engineering Division. We thank the Program of Computational Science and Engineering at UIUC for providing the computing resources.

[1] M. F. Ashby and A. L. Greer, Scr. Mater. **54**, 321 (2006).
[2] J. F. Löffler, Intermetallics **11**, 529 (2003).
[3] J. Schroers and W. L. Johnson, Phys. Rev. Lett. **93**, 255506 (2004).
[4] C. J. Byrne and M. Eldrup, Science **321**, 502 (2008).
[5] Y. Wu, H. Wang, H. H. Wu, Z. Y. Zhang, X. D. Hui, G. L. Chen, D. Ma, X. L. Wang, and Z. P. Lu, Acta Mater. **59**, 2928 (2011).
[6] A. L. Greer, Science **267**, 1947 (1995).
[7] A. I. Salimon, M. F. Ashby, Y. Bréchet, and A. L. Greer, Mat. Sci. Eng. A **375-377**, 385 (2004).
[8] A. Inoue and A. Takeuchi, Acta Mater. **59**, 2243 (2011).
[9] M. M. Trexler and N. N. Thadhani, Prog. Mater. Sci. **55**, 759 (2010).
[10] W. H. Wang, C. Dong, and C. H. Shek, Mater. Sci. Eng. R. **44**, 45 (2004).
[11] D. Xu, G. Duan, and W. L. Johnson, Phys. Rev. Lett. **92**, 245504 (2004).
[12] C. C. Hays, C. P. Kim, and W. L. Johnson, Phys. Rev. Lett. **84**, 2901 (2000).
[13] Q. An, K. Samwer, W. A. Goddard, W. L. Johnson, A. Jaramillo-Botero, G. Garret, and M. D. Demetriou, J. Phys. Chem. Lett. **3**, 3143 (2012).
[14] X. Bai, J. H. Li, Y. Y. Cui, and B. X. Liu, Mater. Lett. **92**, 281 (2013).
[15] C. C. Wang and C. H. Wong, J. Alloys Compd. **510**, 107 (2012).
[16] Y. Zhang, N. Mattern, and J. Eckert, J. Appl. Phys. **111**, 053520 (2012).
[17] Y. Zhang, N. Mattern, and J. Eckert, J. Alloys Compd. **514**, 141 (2012).
[18] L. M. Martinez and C. A. Angell, Nature (London) **410**, 663 (2001).
[19] M. D. Ediger, C. A. Angell, and S. R. Nagel, J. Phys. Chem. **100**, 13200 (1996).

[20] M. D. Ediger, Ann. Rev. Phys. Chem. **51**, 99 (2000).
[21] D. R. Reichman and P. Charbonneau, J. Stat. Mech. (2005) P05013.
[22] D. Chandler and J. P. Garrahan, Ann. Rev. Phys. Chem. **61**, 191 (2010).
[23] V. Lubchenko and P. G. Wolynes, Ann. Rev. Phys. Chem. **58**, 235 (2007).
[24] G. Adam and J. H. Gibbs, J. Chem. Phys. **43**, 139 (1965).
[25] M. H. Cohen and G. S. Grest, Phys. Rev. B **20**, 1077 (1979).
[26] G. Tarjus, S. A. Kivelson, Z. Nussinov, and P. Viot, J. Phys.: Condens. Matter **17**, R1143 (2005).
[27] N. Lačević, F. W. Starr, T. B. Schrøder, and S. C. Glotzer, J. Chem. Phys. **119**, 7372 (2003).
[28] L. Berthier and G. Biroli, Rev. Mod. Phys. **83**, 587 (2011).
[29] C. Dasgupta, A. V. Indrani, S. Ramaswamy, and M. K. Phani, Europhys. Lett. **15**, 307 (1991).
[30] T. R. Kirkpatrick, D. Thirumalai, and P. G. Wolynes, Phys. Rev. A **40**, 1045 (1989).
[31] J. C. Phillips, Rep. Prog. Phys. **59**, 1133 (1996).
[32] R. Böhmer, R. Chamberlin, G. Diezemann, B. Geil, A. Heuer, G. Hinze, S. Kuebler, R. Richert, B. Schiener, H. Sillescu, H. Spiess, U. Tracht, and M. Wilhelm, J. Non-Crystall. Solids **235-237**, 1 (1998).
[33] G. L. Squires, *Introduction to the Theory of Thermal Neutron Scattering* (Cambridge University Press, Cambridge, 2012).
[34] P. Egelstaff, *An Introduction to the Liquid State* (Academic Press, London, 1967).
[35] J.-P. Hansen and I. R. McDonald, *Theory of Simple Liquids*, 3rd ed. (Academic Press, London, 2006).
[36] Y. Q. Cheng, E. Ma, and H. W. Sheng, Phys. Rev. Lett. **102**, 245501 (2009).
[37] N. S. Barekar, S. Pauly, R. B. Kumar, U. Kühn, B. K. Dhindaw, and J. Eckert, Mater. Sc. Eng. A **527**, 5867 (2010).
[38] Y. Zhang, N. Mattern, and J. Eckert, J. Appl. Phys. **110**, 093506 (2011).
[39] Y. Y. Cui, T. L. Wang, J. H. Li, Y. Dai, and B. X. Liu, Phys. Chem. Chem. Phys. **13**, 4103 (2011).
[40] H. Z. Fang, X. Hui, G. L. Chen, and Z. K. Liu, Appl. Phys. Lett. **94**, 091904 (2009).
[41] Y. Q. Cheng and E. Ma, Appl. Phys. Lett. **93**, 051910 (2008).
[42] Y. Q. Cheng, H. W. Sheng, and E. Ma, Phys. Rev. B **78**, 014207 (2008).
[43] J. Hwang, Z. H. Melgarejo, Y. E. Kalay, I. Kalay, M. J. Kramer, D. S. Stone, and P. M. Voyles, Phys. Rev. Lett. **108**, 195505 (2012).
[44] G. Kumar, T. Ohkubo, T. Mukai, and K. Hono, Scr. Mater. **57**, 173 (2007).
[45] C. C. Yuan, X. Shen, J. Cui, L. Gu, R. C. Yu, and X. K. Xi, Appl. Phys. Lett. **101**, 021902 (2012).
[46] J. Ding, Y. Q. Cheng, H. Sheng, and E. Ma, Phys. Rev. B **85**, 060201 (2012).
[47] J. Ding, Y. Q. Cheng, and E. Ma, Acta Mater. **61**, 4474 (2013).
[48] J. Ding, Y. Q. Cheng, and E. Ma, Acta Mater. **69**, 343 (2014).
[49] K. N. Lad, N. Jakse, and A. Pasturel, J. Chem. Phys. **136**, 104509 (2012).
[50] X. J. Han and H. R. Schober, Phys. Rev. B **83**, 224201 (2011).
[51] A. Meyer, J. Wuttke, and W. Petry, J. Non-Crystall. Solids **250-252** (Part 1), 116 (1999).
[52] A. Meyer, J. Wuttke, W. Petry, O. G. Randl, and H. Schober, Phys. Rev. Lett. **80**, 4454 (1998).
[53] A. Meyer, W. Petry, M. Koza, and M. P. Macht, Appl. Phys. Lett. **83**, 3894 (2003).
[54] N. A. Mauro, M. Blodgett, M. L. Johnson, A. J. Vogt, and K. F. Kelton, Nat. Commun. **5**, 1 (2014).
[55] T. Kordel, D. Holland-Moritz, F. Yang, J. Peters, T. Unruh, T. Hansen, and A. Meyer, Phys. Rev. B **83**, 104205 (2011).
[56] S. Plimpton, J. Comp. Phys. **117**, 1 (1995).
[57] L. Ward, A. Agrawal, K. M. Flores, and W. Windl, arXiv:1209.0619.
[58] W. Kob and H. C. Andersen, Phys. Rev. E **52**, 4134 (1995).
[59] T. Egami, Mod. Phys. Lett. B **28**, 1430006 (2014).
[60] A. K. Jain and R. C. Dubes, *Algorithms for Clustering Data*, edited by B. Marttine (Prentice-Hall, Eaglewood Cliffs, NJ, 1988).
[61] *Matlab and Statistics Toolbox Release 2014a* (The MathWorks, Natick, Massachusetts, USA, 2014).
[62] C. Zahn, IEEE Trans. Comp. **C-20**, 68 (1971).
[63] J. B. Kruskal, Proc. Am. Math. Soc. **7**, 48 (1956).
[64] R. C. Prim, Bell Syst. Tech. J. **36**, 1389 (1957).
[65] A. Lumsdaine, L.-Q. Lee, and J. G. Siek, *The Boost Graph Library: User Guide and Reference Manual* (Addison-Wesley Longman, Inc., Boston, MA, USA, 2002).
[66] L. Van Hove, Phys. Rev. **95**, 249 (1954).
[67] G. H. Vineyard, Phys. Rev. **110**, 999 (1958).
[68] S. Sastry, P. G. Debenedetti, and F. H. Stillinger, Nature (London) **393**, 554 (1998).
[69] T. Iwashita, D. M. Nicholson, and T. Egami, Phys. Rev. Lett. **110**, 205504 (2013).
[70] Y. Q. Cheng, E. Ma, and H. W. Sheng, Appl. Phys. Lett. **93**, 111913 (2008).
[71] S. M. Chathoth, B. Damaschke, M. M. Koza, and K. Samwer, Phys. Rev. Lett. **101**, 037801 (2008).
[72] L. Berthier, D. Chandler, and J. P. Garrahan, Europhys. Lett. **69**, 320 (2005).
[73] Y. J. Jung, J. P. Garrahan, and D. Chandler, Phys. Rev. E **69**, 061205 (2004).
[74] S. R. Becker, P. H. Poole, and F. W. Starr, Phys. Rev. Lett. **97**, 055901 (2006).
[75] F. Fernandez-Alonso, F. J. Bermejo, S. E. McLain, J. F. C. Turner, J. J. Molaison, and K. W. Herwig, Phys. Rev. Lett. **98**, 077801 (2007).
[76] V. N. Novikov and A. P. Sokolov, Phys. Rev. E **67**, 031507 (2003).
[77] S.-H. Chen, F. Mallamace, C.-Y. Mou, M. Broccio, C. Corsaro, A. Faraone, and L. Liu, Proc. Natl. Acad. Sci. USA **103**, 12974 (2006).
[78] L. Berthier, Physics **4**, 42 (2011).
[79] P. Kumar, Proc. Natl. Acad. Sci. USA **103**, 12955 (2006).
[80] C. A. Angell, J. Chem. Phys. **57**, 470 (1972).
[81] M. I. Ojovan, Entropy **10**, 334 (2008).
[82] D. Chandler, J. P. Garrahan, R. L. Jack, L. Maibaum, and A. C. Pan, Phys. Rev. E **74**, 051501 (2006).
[83] F. Faupel, M.-P. Macht, H. Mehrer, V. Naundorf, K. Rätzke, H. R. Schober, S. K. Sharma, and H. Teichler, Rev. Mod. Phys. **75**, 237 (2003).
[84] C. Oligschleger and H. R. Schober, Phys. Rev. B **59**, 811 (1999).

[85] M. Kluge and H. R. Schober, Phys. Rev. B **70**, 224209 (2004).
[86] G. S. Matharoo, M. S. Gulam Razul, and P. H. Poole, Phys. Rev. E **74**, 050502(R) (2006).
[87] H. C. Andersen, Proc. Natl. Acad. Sci. USA **102**, 6686 (2005).
[88] B. Vorselaars, A. V. Lyulin, K. Karatasos, and M. A. J. Michels, Phys. Rev. E **75**, 011504 (2007).
[89] D. Caprion, J. Matsui, and H. R. Schober, Phys. Rev. Lett. **85**, 4293 (2000).
[90] S.-H. Chong, Phys. Rev. E **78**, 041501 (2008).
[91] X. Xia and P. G. Wolynes, Phys. Rev. Lett. **86**, 5526 (2001).
[92] W. Kob, C. Donati, S. J. Plimpton, P. H. Poole, and S. C. Glotzer, Phys. Rev. Lett. **79**, 2827 (1997).